Available free online at www.medjchem.com

Mediterranean Journal of Chemistry

Mediterranean Journal of Chemistry **2020**, 10(4), 378-395

Croweacin and *Ammi visnaga* (L.) Lam Essential Oil derivatives as green corrosion inhibitors for brass in 3% NaCl medium: Quantum Mechanics investigation and Molecular Dynamics Simulation Approaches

Anas Chraka [1,*], Ihssane Raissouni [1], Nordin Ben Seddik [1], Said Khayar [1], Soukaina El Amrani [2], Mustapha El Hadri [3], Faiza Chaouket [1] and Dounia Bouchta [1]

[1] Materials and Interfacial Systems Laboratory, ERESI Team. Department of Chemistry, Faculty of Sciences, Abdelmalek Essaadi University, Tetouan, Morocco

[2] Materials, Processes, Catalysis and Environment Laboratory. Higher School of Technology of Fez, Sidi Mohamed Ben Abdellah University, Imouzzer Road, Fez 30000-Morocco

[3] Laboratory of Condensed Matter Physics, Faculty of Sciences, Abdelmalek Essaadi University, Tetouan, Morocco

Abstract: The computational study was carried out to understand the anti-corrosion properties of Croweacin, a major chemical component of two essential oils of *Ammi visnaga* (L.) Lam collected from northern Morocco in 2016 (EO16) and 2018 (EO18) against brass corrosion in a 3% NaCl medium. The study, moreover, considers the inhibitory effect of some minor compounds of EO18 such as Eugenol, Trans-Anethole, α-Isophorone, and Thymol. In this context, the quantum mechanics modelling using the density functional theory (DFT) method with B3LYP /6-31G (d, p) were conducted in the aqueous medium by the use of the IEFPCM model and SCRF theory. The DFT method was adopted to identify, analyze and interpret several elements such as the electronic features, the Frontier Molecular Orbitals (FMO) diagram, Molecular Electrostatic Potential (MEP), contours maps of the electrostatic potential (ESP), and the Mulliken population analysis. The DFT demonstrated that the studied compounds are excellent corrosion inhibitors.

Furthermore, the Monte Carlo (MC) type simulation of molecular dynamics (MD) was carried out to provide information on the adsorption mechanism of the studied inhibitors through the active sites on the metal surface. This method informed us that the studied inhibitors have high adsorption energy when interacting with the metal surface, especially for Croweacin (-68.63 kcal/mol). The results obtained from DFT and the MC type simulations are in good agreement.

Keywords: Croweacin; Monte Carlo; *Ammi visnaga* (L.) Lam; Brass; Corrosion; DFT.

1. Introduction

The serious consequences of the corrosion process have become a problem of global importance. In addition to our daily contact with this form of degradation, corrosion causes depletion of resources, loss or contamination of useful products, and thus, increase the economic costs and environmental risks [1]. Copper and its alloys (brass, bronze, etc.) have been widely used in water and steam systems to manufacture tubes, fittings, fasteners, and various components molded in ocean engineering. Despite its high resistance, this type of metal is very sensitive to corrosion in chloride-containing solutions, i.e. seawater. The presence of Cl^- ions contributes drastically to corrosion mechanism and therefore, the metal dissolution [2]. This serious dilemma dissipates enormous financial resources every year, and thus in a significant economic loss [3,4].

In this context, searching for best protection of Copper and its alloys in a 3% NaCl solution (e.g. seawater) by using effective, economical, non-toxic and above all environmentally friendly inhibitors remains the objective of many chemistry researchers today [5-7]. Essential oils and their compounds have been cited as effective natural inhibitors of metal corrosion in the literature through various researches [8-10]. These natural inhibitors are inexpensive and can be developed to be handy and to

*Corresponding author: Anas Chraka
Email address: anaschraka@gmail.com
DOI: http://dx.doi.org/10.13171/mjc10402004281338ac

Received February 12, 2020
Accepted March 19, 2020
Published April 28, 2020

meet the requirements of the industrial sector [11,12]. These natural corrosion inhibition molecules may form a protective layer by adsorbing on the metal surface via covalent bonds (chemisorption) and/or electrostatic bonds (physisorption) [13]. The corrosion-inhibiting properties of this type of compound are due to the capacity of heteroatoms and the π electrons of the aromatic ring to share electrons with the metal surface, which leads to the formation of a protective film [14,15].

As mentioned earlier, although essential oils are commonly used as green inhibitors in several studies, the understanding of their effect and their corrosion inhibiting mechanisms has not been well clarified. This may be due in part to the presence of many molecules belonging to different chemical families (Monoterpenes, Terpenes, Phenols, Sesquiterpenes, etc.) in essential oils. This makes it challenging to identify the active compound with the inhibitory property. Therefore, we have proposed to use computational chemistry as one of the solutions adopted in this work to solve this problem.

Traditionally, inhibition performance tests are generally performed by the main known electrochemical methods such as polarization curves, electrochemical impedance spectroscopy (EIS) and weight loss. However, all of these techniques are expensive and time-consuming to study the inhibition processes [16]. Currently, computational chemistry is used in all branches of chemistry, including the study of corrosion inhibitors, where it has become the most used tool to understand better the inhibitory power and the interaction mechanisms with the metal surface [17]. This technique has multiple advantages to evaluate the inhibition performance and to explore the inhibition mechanism more precisely and at lower cost [18]. Within the same context, the theory of functional density (DFT), as a theoretical tool, has successfully shown the ability to define with high accuracy the geometric molecular properties, binding energies, as well as assessing the interaction between the inhibitor and the metal surface [19,20]. This theoretical study of corrosion inhibitors is not considered complete unless simulation of molecular dynamics is used to give a more realistic and perfect vision of what is occurring experimentally.

As a part of our ongoing research project, in our recently published paper [21], we discussed the inhibitory performances of two *Ammi visnaga* (L.) lam extracts collected in 2016 (EO16) and 2018 (EO18) on the corrosion of brass in 3% NaCl medium using electrochemical methods. These methods are based on the potentiodynamic polarization curves and electrochemical impedance spectroscopy (EIS). In the same approach, this paper focused on comparing the simulated theoretical results with their experimental counterpart. To this end and towards a better understanding of the inhibitory power of these two oils' components, the inhibitory power of the majority compound (Croweacin) with all the other compounds were analyzed and compared. The aim is to provide satisfactory answers of the studied oils inhibition process through quantum mechanics (QM) modelling in the aqueous phase using DFT- B3LYP/6-31G(d,p) IEFPCM model and with the analysis of the electronic distribution of the studied compounds. Besides, molecular dynamic simulation based on the Monte Carlo (MC) method was adopted to complete the DFT calculations and to look for a logical explanation of the high inhibitory power of EO18 compared to EO16. Besides, since brass was used in the experimental study and because copper constitutes the largest fraction of brass [21], we intended to comprehend the interaction of the studied inhibitors on the surface of copper.

2. Materials and methods

2.1. Quantum mechanics methodology

To get the analysis of the studied compounds electronic features in this work, the quantum mechanics (QM) computations utilizing density functional theory (DFT) were conducted [15,22]. All computational studies were carried out with the Gaussian (09W) program [23]. The optimized geometry was carried using the DFT method in the scheme of the hybrid function of Becke three-parameters; Lee, Yang, and Parr (B3LYP) with the 6-31G(d,p) basic set has been used to provide electronic-structure properties and precise geometries for a large number of organic compounds [24]. The DFT study was done in an aqueous medium using the Integral Equation Formalism Polarizable Continuum (IEFPCM) model and self-consistent reaction field (SCRF) theory [25] to simulate the experimental conditions of the corrosive medium. Since the corrosive medium is neutral, all calculations were performed in the neutral form of the studied molecules. The results obtained were visualized with the Gaussview software [26].

In addition, the electronic-structure parameters analyzed here include the energy of the highest occupied molecular orbital (E_{HOMO}), the energy of the lowest unoccupied molecular orbital (E_{LUMO}), the gap energy (ΔE_{gap}), the ionization potential (I), the electron affinity (A), the dipole moment (μ), the electronegativity (χ), the electrophilicity index (ω), the hardness (η), the softness (σ), and the fraction of electrons transferred (ΔN).

To understand the fraction of electrons transferred (ΔN) between the brass and the inhibitors, we rely on copper (ΔN_{Cu}) because of its high percentage in this alloy (brass) [21]. According to the simple charge transfer by donation and back-donation ($\Delta E_{back\text{-}donation}$) model proposed by Gomez et al. [27], an electronic back-donation process could occur governing the interaction between the inhibitor molecule and the metal surface. The $\Delta E_{back\text{-}donation}$ implies that when $\eta > 0$ and $\Delta E_{back\text{-}donation} < 0$ the charge transfer to a molecule, followed by a back-donation from the molecule, is energetically favored. All these

parameters have been calculated according to equations (1-9) as indicated in the literature [24,3].

$$\Delta E_{gap} = E_{LUMO} - E_{HOMO} \quad (1)$$

$$I = -E_{HOMO} \quad (2)$$

$$A = -E_{LUMO} \quad (3)$$

$$X = \frac{(I + A)}{2} \quad (4)$$

$$\eta = \frac{(I - A)}{2} \quad (5)$$

$$\sigma = \frac{1}{\eta} \quad (6)$$

$$\omega = \frac{X^2}{2\eta} \quad (7)$$

$$\Delta N_{Cu} = \frac{X_{Cu} - X_{inh}}{2(\eta_{Cu} + \eta_{inh})} \quad (8)$$

Where X_{Cu} *= 4,48 eV and* η_{Cu} *= 0 eV* [28].

$$\Delta E_{back-donation} = -\frac{\eta}{4} \quad (9)$$

2.2. Molecular dynamics simulation

Molecular dynamics simulation of the Metropolis Monte Carlo (MC) type implemented using Material Studio 8.0 software from Accelrys Inc. [29] was used to assess the nature of the interaction between the inhibitor and the metal. We built the adsorption system on the surface of copper (Cu (111)), considering that brass is one of its alloys, in addition to being the dominant element of this metal [21]. The selected crystalline surface Cu (111) is the most stable, as the literature had shown [30,31]. For the theoretical study to be homogeneous and sequential, we have extracted the selected inhibitory molecules, which has been studied in its neutral forms in the aqueous medium using DFT at the B3LYP / 6-31G (d, p) level to be used in the simulation system of MC.

The calculations were applied using the COMPASS [32] at 298 K force field to optimize the structures of all system components and represent a technological breakthrough in the force field method. The COMPASS force field is the first ab initio forcefield [33] which allows precise and simultaneous prediction of chemical properties (structural, conformational, vibrational, etc.) including the one in the condensed phase (equation of state, cohesive energies, etc.) for a wide range of chemical systems [17]. The simulation of MC between the inhibitors and the Cu atoms was carried out in a simulation box (20.44×20.44× 38.34Å) with boundary conditions [34]. The Cu (111) surface was constructed from the optimized crystal surface using a 4 x 4 super-cell, and then a 30Å vacuum layer is maintained on the Cu (111) surface.

3. Results and Discussion

3.1. Quantum mechanics results

The use of ab initio QM computations based on DFT was evaluated to comprehensively understand the electrochemical results which showed a best inhibitory effect of EO18 (E = 95.65 (%)) compared to EO16 (E = 85 (%)) [21]. This method allows in-depth analysis of the quantum chemical parameters structures of major molecules (Croweacin and Linalol) and minor compounds (Monoterpenes, Phenols, Phenylpropenes, Terpene Alcohols, Ethyl Alcohols and Sesquiterpenes) of these two EOs [21].

From a quantum chemical point of view, it is known from the literature that adsorption of molecules inhibiting corrosion on a metal surface takes place by means of a donor-acceptor mechanism [35]. Such interaction occurs between sites rich in electrons with an electron-donating capacity, namely heteroatoms, aromatics, and multiple bonds which characterize the inhibitory molecule and the sites poor in electrons with an electron acceptance capacity that characterizes metal atoms on the other hand.

The DFT method used was adapted to rationalize this adsorption mechanism. Thus, we have calculated the electronic parameters such as E_{HOMO}, E_{LUMO}, ΔE_{gap}, and μ. These parameters will provide us with preliminary information of the compounds responsible for the inhibition in EO16 and EO18 (Table 1).

Generally, the donation of electrons and the acceptability of an inhibitory molecule are determined by the Frontier Molecular Orbitals (FMO). The study of the highest occupied molecular orbit (HOMO) and the lowest unoccupied molecular orbit (LUMO) is essential to explain the molecules chemical reactivity. It is known that one of the energy values of the highest occupied molecular orbital (E_{HOMO}) is higher and that the energy of the lowest unoccupied molecular orbital (E_{LUMO}) is lower. This leads the electron transfer tendency to an appropriate acceptor molecule and facilitates adsorption on the metal surface [36]. Furthermore, the difference between these energy levels (ΔE_{gap}) is a vital descriptor depending on the reactivity of the inhibitory molecule regarding the adsorption on the metal surface. The lower is the value of ΔE_{gap} indicate the higher is the reactivity of the inhibitor and thus the excellent adsorption ability [37].

Table 1. Quantum chemical parameters for the studied molecules of EO16 and EO18 in their neutral forms obtained in the aqueous phase with the DFT at the B3LYP/6-31G (d,p) level.

Molecules	E_{HOMO} (eV)	E_{LUMO} (eV)	ΔE_{gap} (eV)	A (eV)	I (eV)	μ (Debye)
EO16						
β- Pinene	-6.31	0.68	6.99	-0.68	6.31	0.93
2-Methylpropyl butanoate	-7.43	0.30	7.64	-0.30	7.43	2.43
Amyl isobutyrate	-7.32	0.28	7.60	-0.28	7.32	2.30
Limonene	-7.71	2.14	9.85	-2.14	7.71	0.80
Isobutyl valerate	-7.46	0.32	7.78	-0.32	7.46	2.43
Linalol	-6.20	0.45	6.65	-0.45	6.20	1.76
γ-Terpinene	-6.00	0.75	6.75	-0.75	6.00	0.06
Menthol	-7.02	2.24	9.26	-2.24	7.02	1.91
2-Methylbutyl 2-methylbutyrate	-7.36	0.27	7.63	-0.27	7.36	2.45
Amyl isovalerate	-7.21	0.47	7.68	-0.47	7.21	1.83
Croweacin	**-5.68**	**0.01**	**5.69**	**-0.01**	**5.68**	**2.08**
Citronellyl isobutyrate	-6.20	0.27	6.47	-0.27	6.20	2.47
EO18						
α-Pinene	-6.00	0.76	6.76	-0.76	6.00	0.24
Linalol	-6.20	0.45	6.65	-0.45	6.20	1.76
α-Isophorone	**-6.54**	**-1.27**	**5.27**	**1.27**	**6.54**	**5.62**
Linalyl valerate	-6.22	0.21	6.43	-0.21	6.22	2.65
Bornyl acetate	-7.21	0.44	7.65	-0.44	7.21	1.91
Thymol	**-5.87**	**0.00**	**5.87**	**0.00**	**5.87**	**1.87**
Geranyl acetate	-6.17	0.29	6.46	-0.29	6.17	2.86
Trans-Anethole	**-5.48**	**-0.62**	**4.86**	**0.62**	**5.48**	**1.87**
Citronellyl propionate	-6.20	0.33	6.53	-0.33	6.20	2.45
Croweacin	**-5.68**	**0.01**	**5.69**	**-0.01**	**5.68**	**2.08**
Eugenol	**-5.61**	**0.07**	**5.68**	**-0.07**	**5.61**	**3.25**
(Z) Farnesyl acetate	-6.05	0.15	6.20	-0.15	6.05	3.17

The results of EO16 compounds (Table 1) revealed that the highest energy EHOMO characterizes the Croweacin = -5.68 eV, the lowest energy $E_{LU\ MO}$ = 0.01eV, and the lowest value of ΔE_{gap} (5.69 eV) compared to other molecules. Thus, Croweacin could perform better as a corrosion inhibitor.

Croweacin revealed to have a large dipole moment value. This latter parameter proved to enhance the adsorption between the Croweacin molecule and the metal surface [38]. In this analysis, we also noted that almost all the EO16 compounds, in addition to the second major compound (Linalol), have high dipole moments. Although the obtained values of the quantum parameters (E_{HOMO}, E_{LUMO} and ΔE_{gap}) for these compounds (Linalool, β- Pinene, Amyl isobutyrate, γ-Terpinene,etc.) are not equivalent to those obtained for Croweacin, it turned out, from this calculation, that EO16 compounds have no inhibitory performance except Croweacin. These results show that he does not always exist a correlation between the dipole moment and the effectiveness of the corrosion inhibition. Some authors have addressed this divergence to which we have referred [39,40].

Considering that the study of the EO18 compounds listed in (Table 1) has shown that there are, in addition to Croweacin, other minor compounds (Trans-Anethole, Eugenol, α-Isophorone, and Thymol) with low values of the energy gap ΔE_{gap} compared to other molecules of the same oil. This indicates that the reactivity of these molecules for the metal surface is fundamentally allowing them to be easily adsorbed on the metal surface, and therefore

enhance the inhibitory efficiency. These same compounds have the lowest values of E_{LUMO} energy, which increases their probability to accept electrons from the metal surface by forming covalent bonds [41].

(Fig.1) presents the Frontier Molecular Orbitals (FMO) diagram of these compounds.

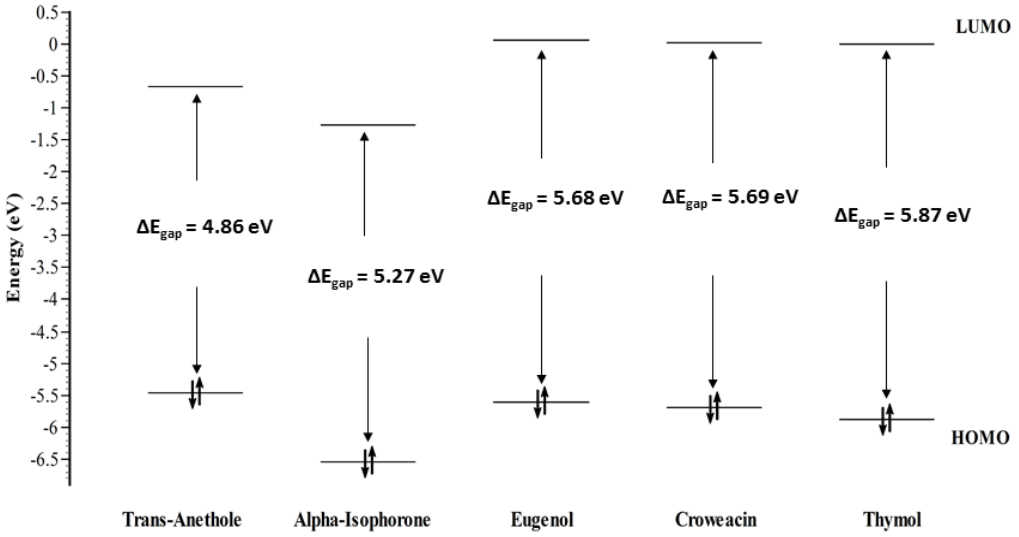

Figure 1. Frontier Molecular Orbitals (FMO) diagram of the selected inhibitors in their neutral forms calculated in the aqueous phase with the DFT at the B3LYP/6-31G(d,p) level.

According to (Fig.1), the value of the ΔE_{gap} decreases according to this order:

Thymol > *Croweacin* ≈ *Eugenol* > *α-Isophorone* > *Trans-Anethole*

Therefore, it can be deduced that these molecules are relatively reactive chemical species; in other words, they are able to share electrons with the metal surface to establish coordination bonds [42]. It can also be noted that there is an insignificant difference in donation capacity, which is slightly higher for Trans-Anethole.

The dipole moment (μ) is an electronic descriptor of a molecule to rationalize its structure. There is, however, no consensus on the correlation between the dipole moment and the corrosion inhibition efficiency [8,43]. There is a view that a high dipole moment promotes high inhibition efficiency, while there is also a dissenting opinion [44,45]. This difference was evident in our EO16 compounds analysis and EO18 results.

The compounds that have shown inhibitory properties in EO18 are characterized by a large value of dipole moment, which is distributed as follows:

α-Isophorone > *Eugenol* > *Croweacin* > *Thymol* ≈ *Trans-Anethole*

However, some EO18 compounds have shown a high dipole moment value, although with the absence of corrosion inhibitors properties. These analyzes confirm the confusion previously described by many researchers on the correlation between μ and the inhibition efficiency. We can, therefore, conclude that the high value of this parameter does not always distinguish the corrosion inhibitor or its relationship with the inhibition efficiency.

According to the studied quantum chemical parameters, it is clear that Croweacin, as a major compound, exhibits characteristics associated with a corrosion inhibitor and therefore responsible for the main inhibition properties of EO16 and EO18. In addition, after analysis of EO18 compounds, it turns out that in addition to the Croweacin, other minor compounds (Trans-Anethole, Eugenol, α-Isophorone and Thymol) have an inhibitory power. Previous research works have already confirmed the inhibitory properties of Trans-Anethole, Eugenol, and Thymol [8,44,46]. This gives us a preliminary idea of assuming that, in addition to Croweacin, these minor compounds are suitable corrosion inhibitors, which enhance the inhibitory capacity of EO18 compared to EO16. To confirm our assumption and show the inhibitory forces of each detected compound, we have calculated other quantum parameters such as electronegativity (χ), electrophilicity index (ω), the hardness (η), the softness (σ), the fraction of electrons transferred (ΔN_{Cu}), and the back donation ($\Delta E_{back\text{-}donation}$) (Table 2).

Table 2. Chemical reactivity indices for the selected inhibitors in their neutral forms calculated in the aqueous phase using DFT at the B3LYP/6-31G(d,p) level.

Quantum parameters	Croweacin	Trans-Anethole	Eugenol	Thymol	α-Isophorone
χ (eV)	2.83	3.05	2.77	2.93	3.90
η (eV)	2.84	2.43	2.84	2.93	2.63
σ (eV^{-1})	0.35	0.41	0.35	0.34	0.38
ω (eV)	1.41	1.91	1.35	1.46	2.89
ΔN_{Cu} (eV)	0.29	0.29	0.30	0.26	0.11
$\Delta E_{back\text{-}donation}$ (eV)	-0.71	-0.60	-0.71	-0.73	-0.65
E_{tot} (a.u)	-651.81	-463.31	-538.52	-464.53	-426.43

Electronegativity (χ) is a factor that determines the electrons attractiveness towards chemical species. This is an important indicator to determine the fraction of the electron transferred from the inhibiting molecule to the metal surface. According to the literature, a good corrosion inhibitor has a low electronegativity value (χ) [47,48]. Table 2 shows the order of the electronegativity of the studied molecules:

α-Isophorone >Trans-Anethole > Thymol > Croweacin > Eugenol

The obtained electronegativity values show that these compounds are useful inhibitors with a preference for Eugenol.

Hardness (η) and softness (σ) are important quantum descriptors for estimating reactivity and molecular stability. According to the principle of HSAB (Hard and Soft Acids Bases) [49], a hard molecule is associated with low basicity which means a low electron-donating ability; while a soft molecule is related to high basicity and a high tendency to donate electrons. This suggests that a higher value of (σ) and a lower value of (η) are associated with a higher capacity of electron donor and therefore, high inhibition efficiency. In our case, the results in (Table 2) show that the values of (η) follow the following sequence:

Thymol ≥ Eugenol ≈ Croweacin > α-Isophorone > Trans-Anethole

These results are consistent with the general belief that hard molecules should have a large energy gap ΔE_{gap} and that a soft molecule should have a low ΔE_{gap} [50]. In our work, the studied compounds are characterized by a low hardness with a preference for Trans-Anethole. They also have the feeblest ΔE_{gap}, normally the inhibitor with the lowest hardness value (hence the highest softness value) should have the highest inhibitory efficacy. Consequently, these results confirm the inhibitory efficacity of these molecules.

As for the values of (σ), the studied structures are classified in descending order as follows:

Trans-Anethole > α-Isophorone > Croweacin ≈ Eugenol ≥ Thymol

This trend shows that these compounds are reactive and have a high absorption capacity on the surface. This is in good agreement with the experimental observation [21].

The inhibition efficiency is also affected by the value of the electrophilicity index (ω). According to several researchers [51,52], a good nucleophile (donor) is characterized by a lower value of (ω). On the other hand, a good electrophile (acceptor) is characterized by a high value of (ω) [53]. Consequently, a molecule with a lower value of (ω) is a good corrosion inhibitor. As for the values of (ω), the studied inhibitors are in descending order as follows:

α-Isophorone > Trans-Anethole > Thymol > Croweacin > Eugenol

The low value of (ω) observed for each of the five studied compounds in the aqueous phase indicates their higher tendency to donate electrons to the metal surface with a preference for Eugenol. These results confirms the inhibitory performance of these compounds, which affirm the experimental results obtained in our previous study [21].

The transfer of electrons occurs from the inhibitor to the surface atoms of the metal when ΔN> 0, and vice versa if ΔN <0 [54]. ΔN_{Cu} has also been calculated for the studied inhibitors (Table 2). The values of ΔN obtained to follow the following sequence:

Eugenol ≈ Croweacin ≈ Trans-Anethole ≥ Thymol > α-Isophorone

These results confirm the high ability of these compounds to donate electrons with a clear preference for Eugenol, Croweacin, Trans-Anethole, and Thymol.

The information obtained from this study has demonstrated that the studied molecules can transfer electrons to the surface of copper and form a coordinate covalent bond. These results are consistent with the Lukovit study [55]. The donation and back-donation ($\Delta E_{back\text{-}donation}$) of charges were also

calculated in this work. This parameter is just to provide information regarding the electronic back-donation process that could occur between the inhibitory molecule and the atoms of metal surface [21]. If $\eta > 0$ and $\Delta E_{back\text{-}donation} < 0$, the electron donation capacity of the molecule on the metal surface increases, which enhances the inhibition efficiency. According to the calculations of $\Delta E_{back\text{-}donation}$ for the studied compounds, they are less than zero (-0.73 at -0.60 eV) these values indicate that these molecules appear to be good inhibitors for corrosion.

The total energy (E_{tot}) calculated by DFT is also another critical parameter. E_{tot} of a system is made up of internal, potential, and kinetic energy. Hohenberg and Kohn [56] have proved that E_{tot} of a system, including that of the numerous physical effects of electrons in the presence of static external potential, is a unique function of the charge density. The minimum value of the total energy functional is the ground state energy of the system. The electronic charge density, which yields this minimum, is then the exact single-particle ground state energy [57]. In our work, the E_{tot} for the studied inhibitors is as follows: -651.81, -538.52, -464.53, -463.31, and -426.43 (a.u) for Croweacin, Eugenol, Thymol, Trans-Anethole, and α-Isophorone respectively. These high negative values of E_{tot}, confirming the inhibitory efficacy for these compounds with a preference for the primary compound (Croweacin).

Through the above and based on the quantum chemical parameters obtained, it is clear that the compound responsible for the inhibition power in EO16 is Croweacin. However, regarding EO18, there is probably a high inhibitory force due to the presence, in addition to the primary compound (Croweacin), the minor compounds (Eugenol, Trans-Anethole, α-Isophorone, Thymol), which enhanced the inhibition efficiency of EO18. These results somewhat explain the electrochemical study obtained in our previous work [21].

3.1.1. Electronic distribution

The chemical structures of the selected inhibitors, in its neutral forms, are presented in (Fig.2).

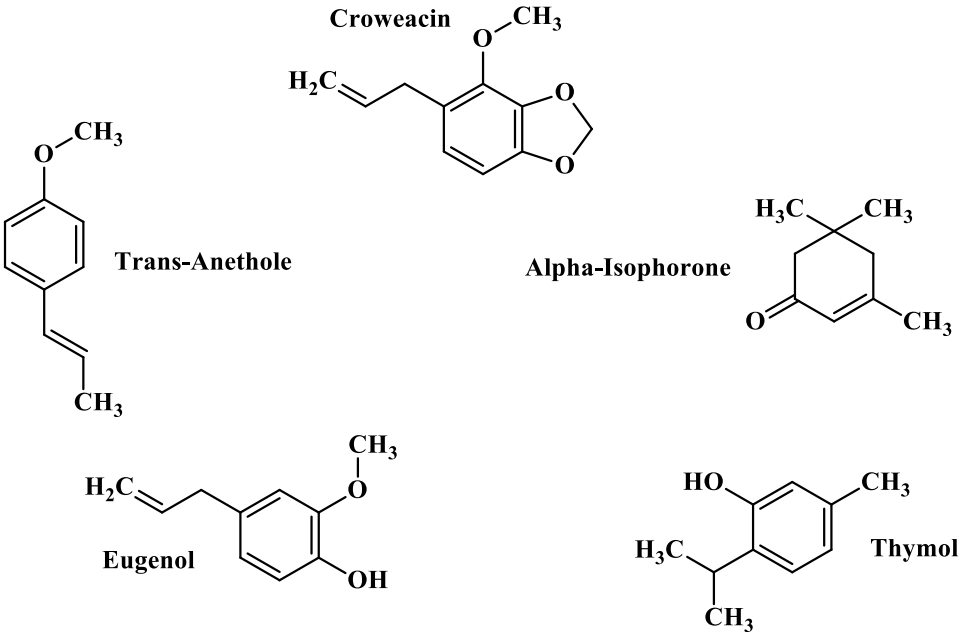

Figure 2. Chemical structures of Croweacin, Trans-Anethole, Eugenol, Thymol, and α-Isophorone in their neutral forms

(Fig.3) presents the HOMO, LUMO and the optimized molecular structures of the studied inhibitors in their neutral forms. It shows that the electronic densities HOMO and LUMO are distributed almost over the entire surface of the studied inhibitors. The positive and negative regions are indicated by the green and red colors, respectively. It is noted that LUMO is distributed over the benzene ring and the carbon atoms. At the same time, the density of HOMO orbital is firmly located over the aromatic cycle and the heteroatoms. This implies that the regions of these molecules develop the strongest tendency to accept and donate electron

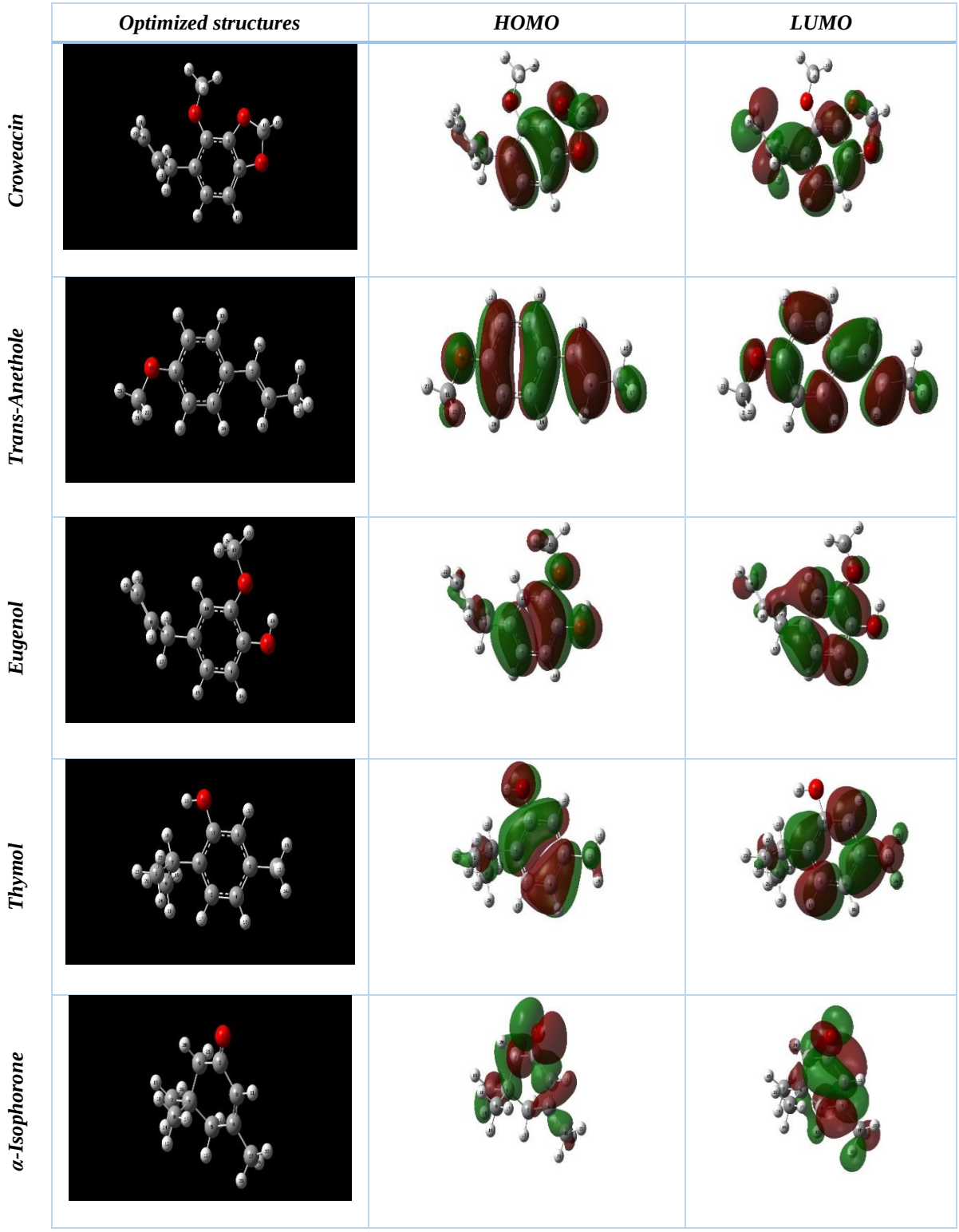

Figure 3. The optimized structures, HOMO and LUMO of the selected inhibitors in their neutral forms obtained in the aqueous phase using DFT at the B3LYP/6-31G (d.p) basis set

3.1.2. Electrostatic potential

Following the above approach concerning the visual representation of the chemically active sites for the studied compounds, (Fig.4) illustrates the molecular electrostatic potential (MEP).

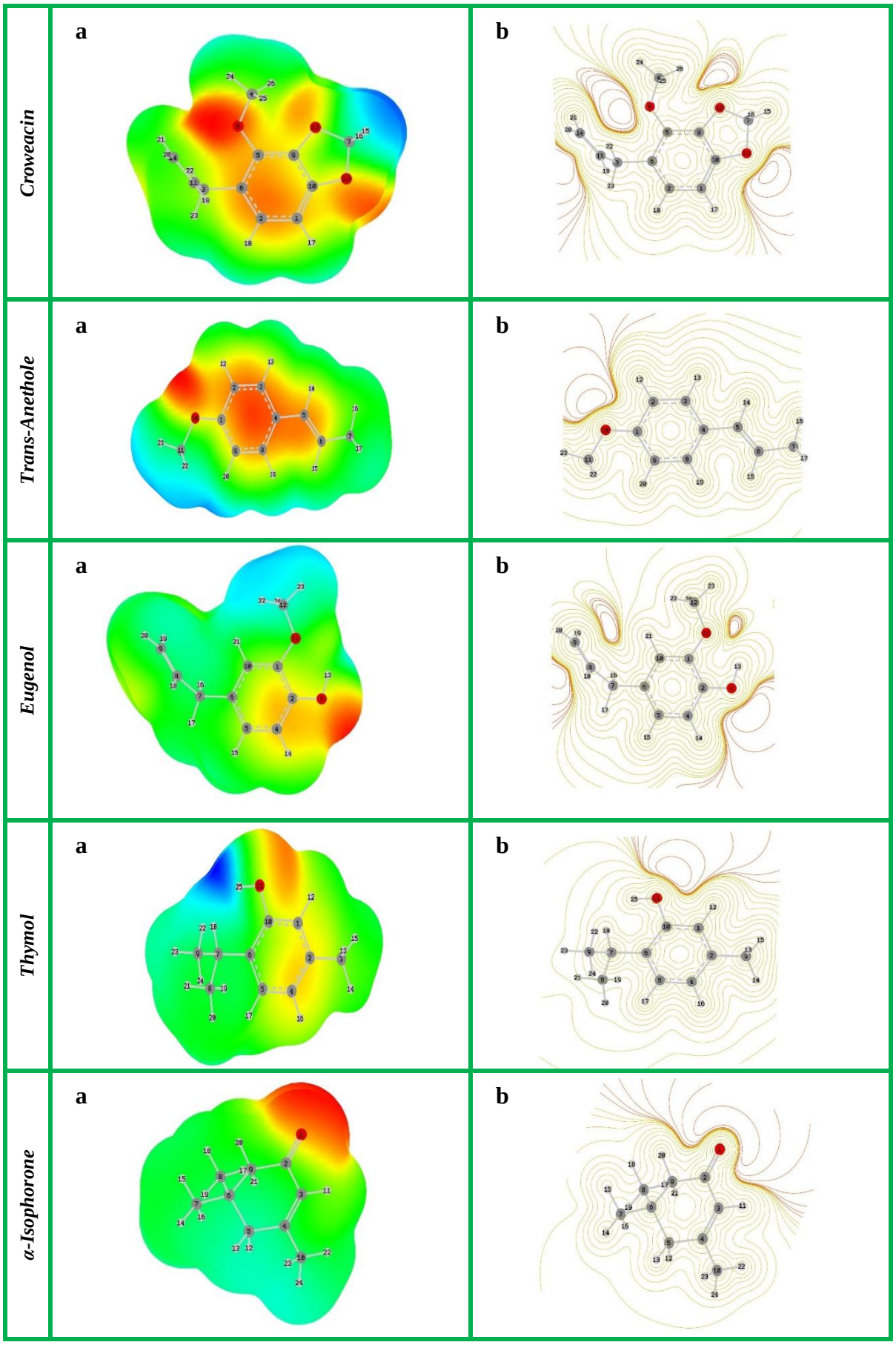

Figure 4. (a) MEP and (b) Contour maps of (ESP) of the selected inhibitors in their neutral forms obtained in the aqueous phase using DFT at the B3LYP/6-31G (d.p) basis set

This tool provides information on the reactive sites for electrophilic and nucleophilic attacks. (Fig.4) shows different values of the electrostatic potential on the surface of the selected inhibitors which are

represented by different colors: red, orange, and yellow representing regions with most negative electrostatic potential related to electrophilic attack, while light blue - blue represents regions with positive electrostatic potential are favorable for nucleophilic attack [58]. On the other hand, the green color represents the region of zero potential. It can be seen that the negatively charged areas (nucleophiles) are located in the benzene rings and the heteroatoms. These electron-rich sites are the preferred sites for adsorption on metallic surfaces [59]. In addition, the same figure presents the outline of the electrostatic potential (ESP) of the studied compounds. It shows that the contour maps of ESP for all inhibitors is present on the surface of aromatic rings and also on heteroatoms (oxygen atoms). This indicates that these molecules are adsorbed in a plane way on the surface of the metal substrate [60].

3.1.3. Mulliken population analysis

From our results discussed above (the quantum chemical parameters, the molecular electrostatic potential (MEP), and the contour maps of the electrostatic potential (ESP)), we could conclude that the studied molecules are more sensitive to the acceptation and donation of electrons than the atoms of the surface metal. Therefore, to support the experimental results [21], it will be beneficial to identify the most reactive sites in these selected inhibitors. The Mulliken atomic charges are used to provide assistance to the active sites of nucleophilic and electrophilic attacks. The Mulliken atoms charges calculated for the studied inhibitors are presented in (Table 3).

Table 3. Mulliken atoms charges for the selected inhibitors in their neutral forms calculated in the aqueous phase using DFT at the B3LYP/6-31G (d.p) basis set.

Croweacin		**Trans-Anethole**		**Eugenol**		**Thymol**		**α-Isophorone**	
Atom	Mulliken charge	Atom	Mulliken charge	Atom	Mulliken charge	Atom	Mulliken charge	Atom	Mulliken charge
C (1)	-0.139	**C (1)**	0.343	**C (1)**	0.328	**C (1)**	-0.153	**O (1)**	-0.548
C (2)	-0.166	**C (2)**	-0.134	**C (2)**	0.282	**C (2)**	0.107	**C (2)**	0.416
C (3)	-0.266	**C (3)**	-0.159	**O (3)**	-0.590	**C (3)**	-0.385	**C (3)**	-0.163
C (4)	-0.090	**C (4)**	0.121	**C (4)**	-0.129	**C (4)**	-0.144	**C (4)**	0.133
C (5)	0.277	**C (5)**	-0.122	**C (5)**	-0.162	**C (5)**	-0.151	**C (5)**	-0.220
C (6)	0.052	**C (6)**	-0.086	**C (6)**	0.094	**C (6)**	0.111	**C (6)**	-0.010
C (7)	0.280	**C (7)**	-0.361	**C (7)**	-0.277	**C (7)**	-0.144	**C (7)**	-0.311
O (8)	-0.547	**C (8)**	-0.157	**C (8)**	-0.022	**C (8)**	-0.310	**C (8)**	-0.312
C (9)	0.288	**C (9)**	-0.147	**C (9)**	-0.268	**C (9)**	-0.303	**C (9)**	-0.240
C (10)	0.308	**O (10)**	-0.534	**C (10)**	-0.174	**C (10)**	0.245	**C (10)**	-0.381
C (11)	-0.018	**C (11)**	-0.092	**O (11)**	-0.565	**O (11)**	-0.586	****	****
O (12)	-0.557	**	****	**C (12)**	-0.088	**	****	**	****
O (13)	-0.552	**	****	**	****	**	****	**	****
C (14)	-0.263	**	****	**	****	**	****	**	****

The examination of these results shows that all heteroatoms (O) and some carbon atoms (benzene rings, and double bonds) have negative charges with high electron density. These atoms, therefore, behave like nucleophilic centers when they interact with the metal surface to form coordinate bond [61]. In this context, it is shown for the Croweacin that the most negative charges are found on of the double bonds and oxygen atoms (C1, C2, C14, O8, O12, and O13). Concerning Trans-Anethole and based on the data in (Table 3), the most negative charges are found on the oxygen atom (O10). Thus some carbon atoms of the aromatic ring carry the most negative charges (C2, C3, C8, and C9). Moreover, and considering Eugenol, the negative charges appeared mainly on the C = C double bonds (C4, C5, C10 and C9) and the two oxygen atoms (O3 and O11). Regarding Thymol, the oxygen atom (O11) and the aromatic ring carbon atoms represent the most negative charges. Finally, the largest negative values are located on the atoms (O1, C3, C5, and C9) for the α-Isophorone.

On the other hand, the most positive charges are located in the remaining carbon atoms of these

inhibitors representing the sites through which nucleophiles can attack. These inhibitors can, therefore, accept electrons from the metal through these atoms [62].

Consequently, the analysis of the Mulliken atoms charges of these inhibitors in their neutral forms showed that these molecules, through these active adsorption sites, probably form a barrier preventing the aggressive ions from interacting with the metal surface, reducing as such the rate of corrosion.

3.2. Molecular dynamic simulation study

The studies of quantum chemical parameters, MEP, the contour maps of (ESP) and the Mulliken population analysis alone are not sufficient to predict the performance of the studied inhibitors despite their success in exploring their mechanism of action.

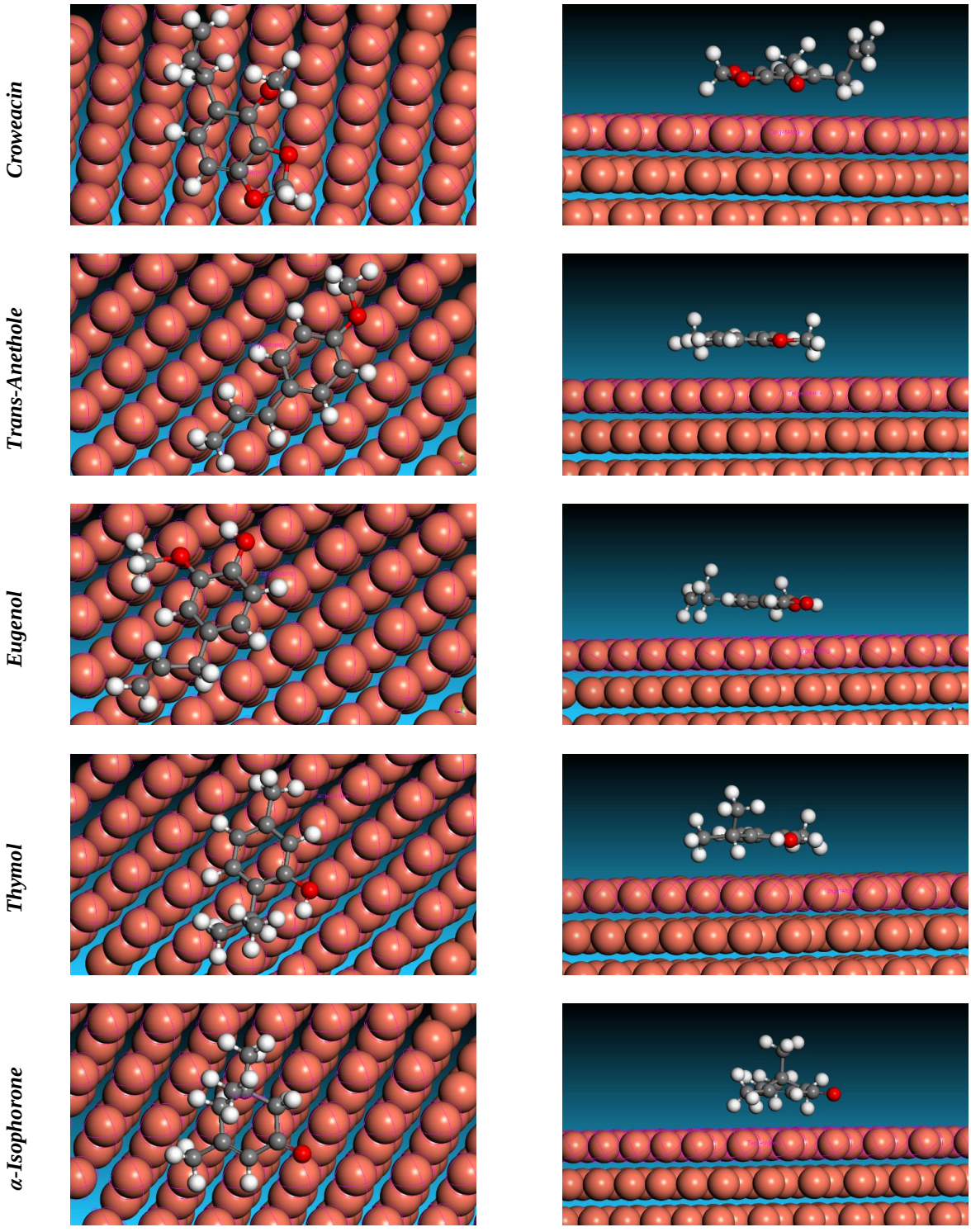

Figure 5. Side and top views of equilibrium adsorption configurations for Cu (111)/ inhibitors systems obtained using the MC simulations

Therefore, we used the Monte Carlo (MC) type simulation of molecular dynamics (MD) to clarify the interaction between these inhibitors in their neutral forms and the copper surface [21], as well as to understand better the inhibitory properties of these inhibitors, which could have given EO18 high inhibiting power compared to EO16.

The system reaches equilibrium only if both the temperature and the energy reach a balance [63]. The final equilibrium structures and most stable low-energy configuration of Croweacin; Trans-Anethole; Eugenol; Thymol, and α-Isophorone over the metal surface (i.e., Cu (111)) were studied in (Fig.5) using the simulation of MC.

The examination of this figure clearly shows that there are strong interactions between the studied inhibitory molecules in their neutral forms and the Cu atoms. It is clear from (Fig.5) that the inhibitors were able to adsorb on the surface with parallel orientation. This mode of adsorption can be attributed to the strong interaction between the aromatic rings and the heteroatoms (O) of these studied inhibitors and the metallic surface.

(Fig.6) presents the probability distribution curves for the adsorption energies of the studied inhibitors during the energy optimization process at 298 K. It can be seen that the distribution curves for the adsorption energies for all inhibitors fluctuating throughout the simulation are slight. This can serve as an indication for the system to reach the equilibrium state [64].

As observed in the same figure, it is evident that all the studied compounds have negative energy which is as follows: -68.63; -55.10; -52.77; -46.69; and -44.57 (kcal/mol) for Croweacin; Trans-Anethole; Eugenol; Thymol, and α-Isophorone respectively. We note an apparent preference for the major compound (Croweacin) which has higher negative adsorption energy when interacting with the copper surface. The adsorption energies with negative values testify to the adsorption of inhibitive compounds onto the metal surface [18,15]. These results confirm the inhibitory power of Croweacin and the other minor compounds.

Croweacin

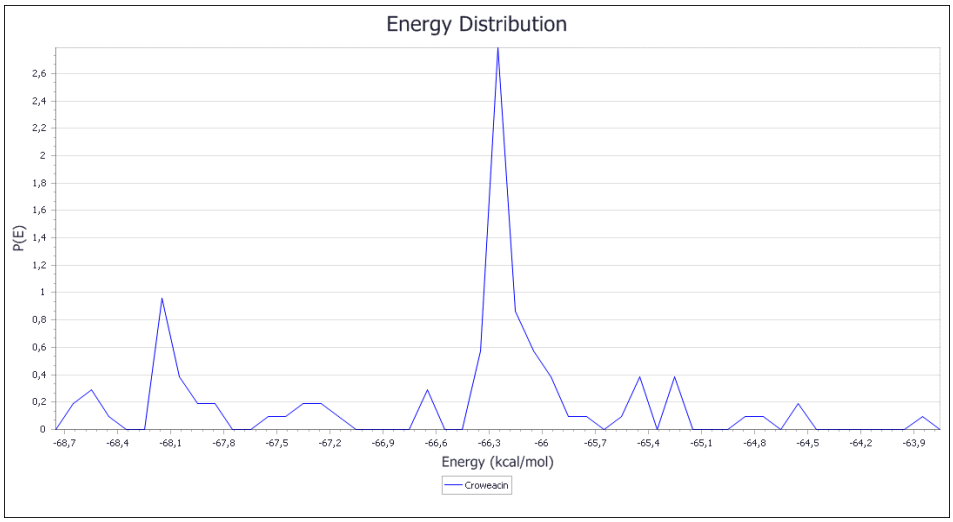

Trans-Anethole

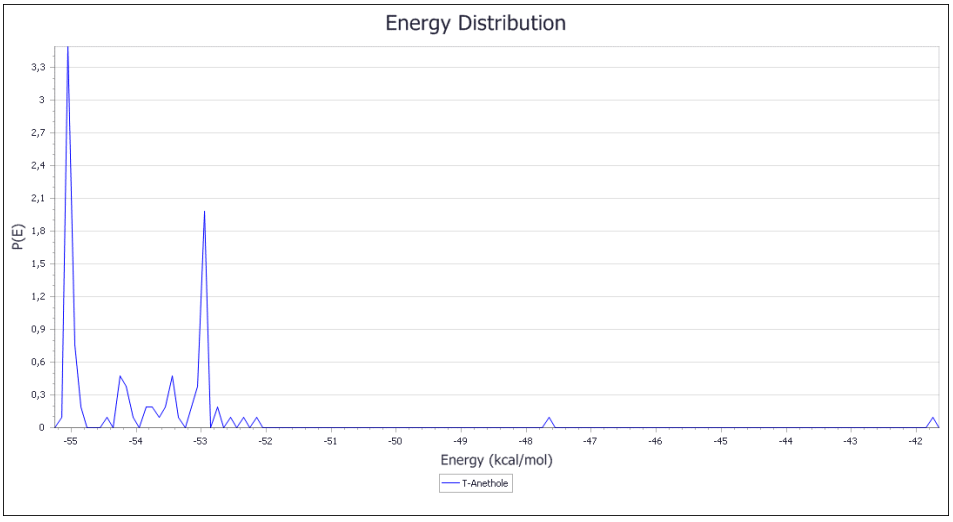

Eugenol

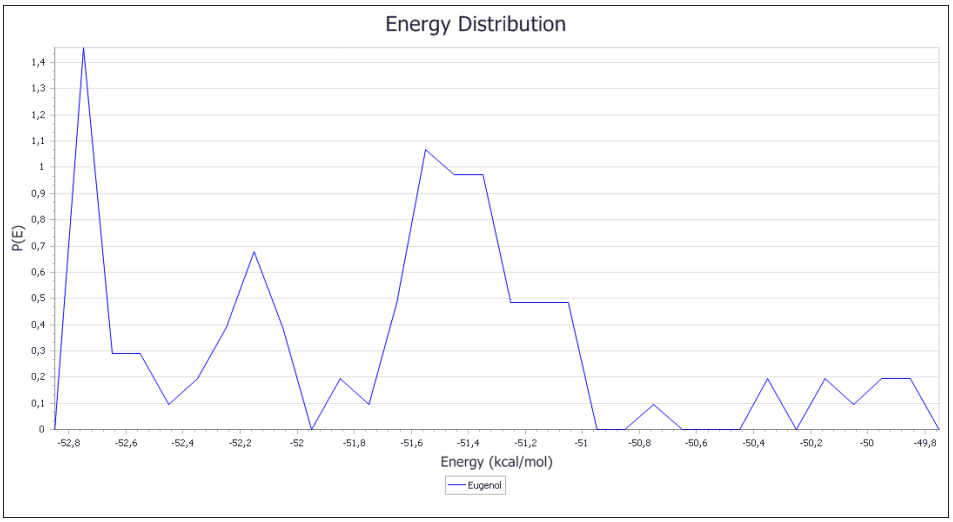

Thymol

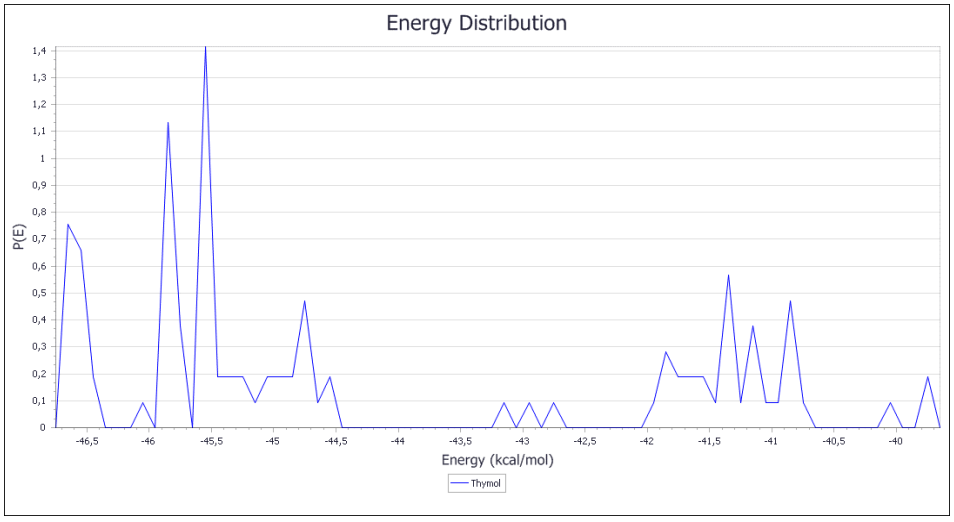

α-Isophorone

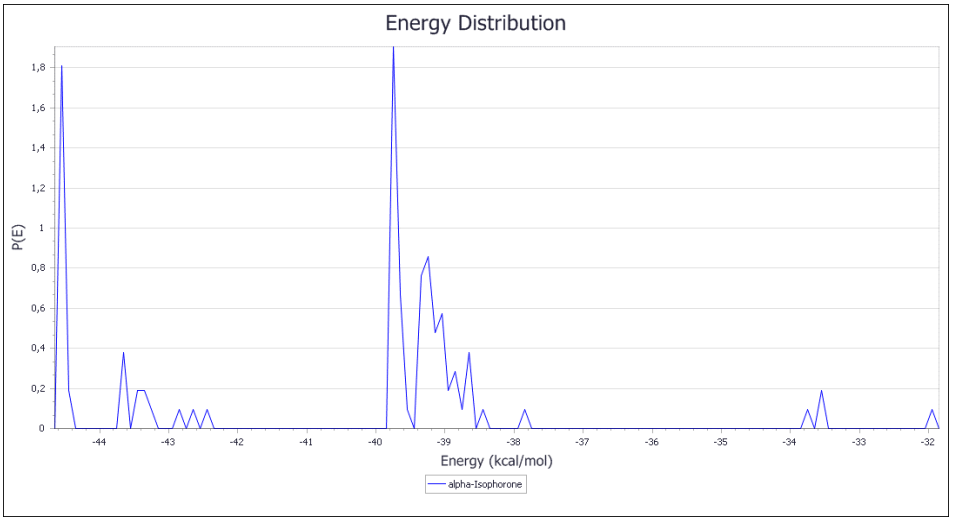

Figure 6. Adsorption energy distribution for Cu (111)/inhibitors systems obtained from MC

Following the above discussion, the different energies of the simulated systems have been calculated and the results obtained are grouped in (Table 4). In the calculations carried out, it was considered that the energy of the substrate (surface of the Copper) is equal to zero. Total energy (E_T) is defined as the sum of the energies of the adsorbed compounds. The adsorption energy (E_{ads}) is the energy required for the compound to be adsorbed on the metal surface. In addition, the adsorption energy reports the energy released (or expected) when the relaxed adsorbate component was adsorbed on the substrate. E_{ads} is defined as the sum of the rigid adsorption energy (E_{Rigid}) and the deformation energy (E_{def}) for the adsorbate compounds. E_{Rigid} reports the energy released (or required) when the non-relaxed adsorbed compounds (i.e. before the geometry optimization step) are adsorbed on the substrate. E_{def} refers to the energy released when the adsorbed adsorbate compounds are relaxed on the surface of the substrate. (Table 4) shows (dE_{ads}/dN_i), which is the energy of the substrate–adsorbate configurations where one of the components of the adsorbate has been removed [17]. According to the simulation process, the studied inhibitors give the maximum energies of adsorption in a negative value (Table 4). The examination of the results shows that the E_{ads} values of the five inhibitors on the surface are respectively -44.57; -46.69; -52.77; -55.10; and -68.63 (kcal/mol) for α-Isophorone, Thymol, Eugenol, Trans-Anethole and Croweacin respectively. The negative apex of E_{ads} indicates that the adsorption of these inhibitors on the surface is spontaneous, powerful, and stable with a clear preference for Croweacin with the rest of the compounds because it has higher negative adsorption energy.

Table 4. The energetic outputs and descriptors obtained from MC simulations of neutral inhibitors over the Cu (111) substrate. (All values are given in Kcal/mol).

Systems	E_T	E_{ads}	E_{Rigid}	E_{def}	dE_{ads}/dN_i (Inhibitors)
Cu (1 1 1) / Croweacin	-33.51	-68.63	-56.95	-11.68	-68.63
Cu (1 1 1) / Trans-Anethole	-40.67	-55.10	-51.41	-3.69	-55.10
Cu (1 1 1) / Eugenol	-46.25	-52.77	-51.11	-1.66	-52.77
Cu (1 1 1) / Thymol	-64.08	-46.69	-46.42	-0.27	-46.69
Cu (1 1 1) / α-Isophorone	-119.31	-44.57	-42.31	-2.26	-44.57

To better understand the inhibitory performances of these studied compounds, we compared their adsorption energies with other inhibitors published in previous researches that studied their inhibitory effects on copper corrosion using the Molecular dynamics simulations.

Awad et al. [65] have reported that neutral forms compound 5-AMT, 5-AMeTT, 1-AMeTT and 5-ATA act as good inhibitors of copper corrosion. The results of the Molecular dynamics simulations for these inhibitors have shown that a flat orientation adsorbs them and the values of the adsorption energy were respectively -30.405, -32.582, -29.071 and

-22.966 (kcal/mol) for 5-AMT, 5-AMeTT, 1-AMeTT and 5-ATA. Our results are in good agreement with Awad et al. [65] results, and our inhibitors have the same direction of absorption on the copper surface. Moreover, the absorption energy values of 5-AMT, 5-AMeTT, 1-AMeTT and 5-ATA were negative and somewhat close to the values of Thymol and α-Isophorone, but lower compared to the values of Croweacin, Eugenol, and trans–Anethole. These comparisons guarantee that all studied compounds in this paper are also good inhibitors.

All the above results confirm that Croweacin is responsible for the corrosion inhibition power in EO16 and EO18, and probably the inhibitory capacity of the minor compounds (α-Isophorone, Thymol, Eugenol, and Trans-Anethole) help Croweacin to give EO18 a high inhibitory power. These results are in good agreement with the experimental outcomes obtained in our previous work [21], as well as the quantum chemical calculations (i.e. DFT).

To confirm the above results and for a more in-depth study concerning the adsorption of these compounds on the metal surface, we analyzed the bond lengths between the heteroatoms of these inhibitors and the surface after stimulation of MC (Table 5). As indicated in the literature, the shortest bond distances between active centers (O) and metal atoms were less than 3.5Å showing the formation of a strong chemical bond (Chemisorption) between these atoms [14], while the bond distance more than 3.5Å indicates that the Van-der-Waals type interaction (physisorption) [66]. Thus, the bond distances calculated for the heteroatoms formed by these studied inhibitors is less than 3.5Å, suggesting that the chemical adsorption could be the crucial role in this inhibition process.

Table 5. Bond lengths values between the selected inhibitors in their neutral forms and Cu (111) surface after molecular adsorption.

Inhibitors	Bond length
Croweacin	do_8 = 2.788 do_{12} = 2.941 do_{13} = 3.033
Trans-Anethole	do_{10} = 2.866
Eugenol	do_3 = 2.994 do_{11} = 2.929
Thymol	do_{11} = 2.978
α-Isophorone	do_1 = 3.015

These results (Table 5) confirm the high inhibitory capacities of the major (Croweacin) and minor (Trans-Anethole, Eugenol, Thymol and α-Isophorone) compounds. Therefore, Croweacin remains the main compound responsible for corrosion inhibition in these two extracts. The high inhibition efficiency of the EOs, mainly for EO18, can be attributed to the adhesion of these inhibitors (Croweacin, Trans-Anethole, Eugenol, Thymol and α-Isophorone) to the metal surface by numerous heteroatoms and double bonds. These later contribute to the formation of strong chemical bonds with the metal surface, which leads to the creation of a secure protective layer. This phenomenon offers a rapid increase in the effectiveness of the major inhibitor (Croweacin) as shown in the experimental results of EO18 [23].

4. Conclusion

This work confirms that theoretical studies can provide a comprehensive understanding of the anti-corrosion properties of Essential Oil. In this paper, the molecular and electronic properties of our inhibitors (Croweacin, Trans-Anethole, Eugenol, α-Isophorone and Thymol) identified by DFT demonstrated the existence of a correlation between the molecular structure of the studied inhibitors and their inhibitory power. Mulliken atomic charges have also shown that the oxygen atoms and some carbon atoms in the aromatic ring and double bonds are active centers for adsorption on the metal surface.

Monte Carlo simulation studies have shown that the studied inhibitors have high adsorption energy when interacting with the copper surface, especially for the major compound (Croweacin). It also gave us an idea of the possible synergistic phenomenon within these studied inhibitors and the metal surface, explaining the high efficiency of EO18 over EO16. Moreover, these methods revealed that the adsorption of these studied inhibitors is occurring via chemisorption.

The results above from two different fields, the first based on quantum mechanics (QM) calculation with density functional theory (DFT) and the second based on classical physics (the simulation of (MC)) are in good agreement.

Finally, this study allowed us to discover a new and good green inhibitor namely Croweacin, which was not previously reported as a corrosion inhibitor at the limit of the authors knowledge.

References

1- S. Aribo, S. J. Olusegun, L. J. Ibhadiyi, A. Oyetunji, D. O. Folorunso, Green inhibitors for corrosion protection in acidizing oilfield environment, Journal of the Association of Arab Universities for Basic and Applied Sciences, **2017**, 24, 34-38.
2- N. Cao, Y. Miao, D. Zhang, R. Boukherroub, X. Lin, H. Ju, H. Li, Preparation of mussel-inspired perfluorinated polydopamine film on brass substrates: Superhydrophobic and anti-corrosion application, Progress in Organic Coatings, **2018**, 125, 109-118.
3- S. A. Haddadi, E. Alibakhshi, G. Bahlakeh, B. Ramezanzadeh, M. Mahdavian, A detailed atomic level computational and electrochemical exploration of the Juglans regia green fruit shell extract as a sustainable and highly efficient green corrosion inhibitor for mild steel in 3.5 wt% NaCl solution, Journal of Molecular Liquids, **2019**, 284, 682-699.
4- H. Cen, Z. Chen, X. Guo, N, S co-doped carbon dots as effective corrosion inhibitor for carbon steel in CO_2-saturated 3.5% NaCl solution, Journal of the Taiwan Institute of Chemical Engineers, **2019**, 99, 224-238.
5- N. B. Seddik, I. Raissouni, K. Draoui, A. A. Aghzzaf, A. Chraka, B. Aznag, F. Chaouket, D. Bouchta, Calcite, the main corrosion inhibitor contained in the raw clay (Rhassoul) of brass in 3% NaCl medium, Mediterranean Journal of Chemistry, **2019**, 9, 236-248.
6- N. B. Seddik, I. Raissouni, K. Draoui, A. A. Aghzzaf, A. Chraka, B. Aznag, F. Chaouket, D. Bouchta, Anticorrosive performance of lanthanum ions intercalated Stevensite clay on brass in 3% NaCl medium, Materials Today: Proceedings, **2020**, 22, 78-82.
7- P. Refait, C. Rahal, M. Masmoudi, Corrosion inhibition of copper in 0.5 M NaCl solutions by aqueous and hydrolysis acid extracts of olive

leaf. Journal of Electroanalytical Chemistry, **2020**, 859, 113834.
8- A. Bouoidina, F. El-Hajjaji, A. Abdellaoui, Z. Rais, M. F. Baba, M. Chaouch, O. Karzazi, A. Lahkimi, M. Taleb,Theoretical and Experimental study of the corrosion inhibition of mild steel in acid medium using some surfactants of the essential oil of FoeniculumVulgare bulb, Journal of Materials and Environmental Sciences, **2017**, 8, 1328-1339.
9- M. Manssouri, A. Laghchimi, A. Ansari, M. Znini, Z. Lakbaibi, Y. El Ouadi, M. Lhou, Effect of Santolina pectinata (Lag.) Essential Oil to protect against the corrosion of Mild steel in 1.0 M HCl: Experimental and quantum chemical studies, Mediterranean Journal of Chemistry, **2020** , 10, 253-68.
10- K. Boumhara, M. Tabyaoui, C. Jama, F. Bentiss, Artemisia Mesatlantica essential oil as green inhibitor for carbon steel corrosion in 1 M HCl solution: Electrochemical and XPS investigations, Journal of Industrial and Engineering Chemistry, **2015**, 29, 146-155.
11- Y. Ye, D. Yang, H. Chen, A green and effective corrosion inhibitor of functionalized carbon dots, Journal of Materials Science & Technology, **2019**, 35, 2243-2253.
12- Y. Ye, Z. Jiang, Y. Zou, H. Chen, S. Guo, Q. Yang, L. Chen, Evaluation of the inhibition behavior of carbon dots on carbon steel in HCl and NaCl solutions, Journal of Materials Science & Technology, **2020**, 43, 144-153.
13- M. Behpour, S. Ghoreishi, N. Soltani, M. Salavati-Niasari, M. Hamadanian, A. Gandomi, Electrochemical and theoretical investigation on the corrosion inhibition of mild steel by thiosalicylaldehyde derivatives in hydrochloric acid solution, Corrosion Science, **2008**, 50, 2172-2181.
14- F. El-Hajjaji, M. Messali, A. Aljuhani, M. Aouad, B. Hammouti, M. Belghiti, D. Chauhan, M. Quraishi, Pyridazinium-based ionic liquids as novel and green corrosion inhibitors of carbon steel in acid medium: electrochemical and molecular dynamics simulation studies, Journal of Molecular Liquids, **2018**, 249, 997-1008.
15- E. Alibakhshi, M. Ramezanzadeh, G. Bahlakeh, B. Ramezanzadeh, M. Mahdavian, M. Motamedi, Glycyrrhiza glabra leaves extract as a green corrosion inhibitor for mild steel in 1M hydrochloric acid solution: experimental, molecular dynamics, Monte Carlo and quantum mechanics study, Journal of Molecular Liquids, **2018**, 255, 185-198.
16- Y. Ye, D. Yang, H. Chen, S. Guo, Q. Yang, L. Chen, H. Zhao, L. Wang, A high-efficiency corrosion inhibitor of N-doped citric acid-based carbon dots for mild steel in hydrochloric acid environment, Journal of hazardous materials, **2020**, 381, 121019.
17- C. Verma, H. Lgaz, D. Verma, E. E. Ebenso, I. Bahadur, M. Quraishi, Molecular dynamics and Monte Carlo simulations as powerful tools for study of interfacial adsorption behavior of corrosion inhibitors in aqueous phase: a review, Journal of Molecular Liquids, **2018**, 260, 99-120.
18- S. K. Saha, P. Ghosh, A. Hens, N. C. Murmu, P. Banerjee, Density functional theory and molecular dynamics simulation study on corrosion inhibition performance of mild steel by mercapto-quinoline Schiff base corrosion inhibitor, Physica E: Low-dimensional systems and nanostructures, **2015**, 66, 332-341.
19- C. Verma, M. A. Quraishi, E. E. Ebenso, I. Bahadur, A Green and Sustainable Approach for Mild Steel Acidic Corrosion Inhibition Using Leaves Extract: Experimental and DFT Studies, Journal of Bio- and Tribo-Corrosion, **2018**, 4, 33.
20- C. Verma, I. B. Obot, I. Bahadur, E.-S. M. Sherif, E. E. Ebenso, Choline based ionic liquids as sustainable corrosion inhibitors on mild steel surface in acidic medium: Gravimetric, electrochemical, surface morphology, DFT and Monte Carlo simulation studies, Applied Surface Science, **2018**, 457, 134-149.
21- A. Chraka, I. Raissouni, N. Benseddik, S. Khayar, A. Ibn Mansour, H. Belcadi, F. Chaouket, D. Bouchta, Aging time effect of *Ammi visnaga* (L.) lam essential oil on the chemical composition and corrosion inhibition of brass in 3% NaCl medium. Experimental and theoretical studies, Materials Today: Proceedings, **2020**, 22, 83-88.
22- S. A. Haddadi, E. Alibakhshi, G. Bahlakeh, B. Ramezanzadeh, M. Mahdavian, A detailed atomic level computational and electrochemical exploration of the Juglans regia green fruit shell extract as a sustainable and highly efficient green corrosion inhibitor for mild steel in 3.5 wt% NaCl solution, Journal of Molecular Liquids, **2019**, 284, 682-699.
23- M. Frisch, G. Trucks, H. Schlegel, G. Scuseria, M. Robb, J. Cheeseman, J. Montgomery, T. Vreven, K. Kudin, J. Burant, Gaussian 09, revision B. 01, Gaussian, Inc., Wallingford CT, 2009 Search PubMed;(b) NM O'Boyle, AL Tenderholt and KM Langner, J. Comput. Chem., **2008**, 29, 839.
24- K. O. Sulaiman, A. T. Onawole, O. Faye, D. T. Shuaib, Understanding the corrosion inhibition of mild steel by selected green compounds using chemical quantum based assessments and molecular dynamics simulations, Journal of Molecular Liquids, **2019**, 279, 342-350.
25- J. Tomasi, B. Mennucci, R. Cammi, Quantum mechanical continuum solvation models, Chemical reviews, **2005**, 105, 2999-3094.
26- A. Frisch, A. Nielson, A. Holder, Gaussview user manual, Gaussian Inc., Pittsburgh, PA, **2000**, 556.
27- B. Gomez, N. Likhanova, M. Dominguez-Aguilar, R. Martinez-Palou, A. Vela, J. L.

Gazquez, Quantum chemical study of the inhibitive properties of 2-pyridyl-azoles, The Journal of Physical Chemistry B, **2006**, 110, 8928-8934.
28- R. G. Pearson, Absolute electronegativity and hardness: application to inorganic chemistry, Inorganic chemistry, **1988**, 27, 734-740.
29- D. Frenkel, B. Smit, Understanding molecular simulation: From algorithms to applications, Elsevier, **2002**, 1, 1-638.
30- N. Kovačević, I. Milošev, A. Kokalj, The roles of mercapto, benzene, and methyl groups in the corrosion inhibition of imidazoles on copper: II. Inhibitor–copper bonding, Corrosion Science, **2015**, 98, 457-470.
31- S. Kaya, B. Tüzün, C. Kaya, I. B. Obot, Determination of corrosion inhibition effects of amino acids: quantum chemical and molecular dynamic simulation study, Journal of the Taiwan Institute of Chemical Engineers, **2016**, 58, 528-535.
32- H. Sun, P. Ren, J. Fried, The COMPASS force field: parameterization and validation for phosphazenes, Computational and Theoretical Polymer Science, **1998**, 8, 229-246.
33- H. Sun, COMPASS: an ab initio force-field optimized for condensed-phase applications overview with details on alkane and benzene compounds, The Journal of Physical Chemistry B, **1998**, 102, 7338-7364.
34- H. C. Andersen, Molecular dynamics simulations at constant pressure and/or temperature, The Journal of chemical physics, **1980**, 72, 2384-2393.
35- S. John, J. Joy, M. Prajila, A. Joseph, Electrochemical, quantum chemical, and molecular dynamics studies on the interaction of 4-amino-4H, 3, 5-di (methoxy)-1, 2, 4-triazole (ATD), BATD, and DBATD on copper metal in 1N H_2SO_4, Materials and Corrosion, **2011**, 62, 1031-1041.
36- N. Asadi, M. Ramezanzadeh, G. Bahlakeh, B. Ramezanzadeh, Utilizing Lemon Balm extract as an effective green corrosion inhibitor for mild steel in 1M HCl solution: a detailed experimental, molecular dynamics, Monte Carlo and quantum mechanics study, Journal of the Taiwan Institute of Chemical Engineers, **2019**, 95, 252-272.
37- D. K. Yadav, B. Maiti, M. Quraishi, Electrochemical and quantum chemical studies of 3, 4-dihydropyrimidin-2 (1H)-ones as corrosion inhibitors for mild steel in hydrochloric acid solution, Corrosion Science, **2010**, 52, 3586-3598.
38- M. Masoud, M. Awad, M. Shaker, M. El-Tahawy, The role of structural chemistry in the inhibitive performance of some amino pyrimidines on the corrosion of steel, Corrosion Science, **2010**, 52, 2387-2396.
39- G. Gao, C. Liang, Electrochemical and DFT studies of β-amino-alcohols as corrosion inhibitors for brass, Electrochimica Acta, **2007**, 52, 4554-4559.
40- H. Tanak, A. Ağar, M. Yavuz, Experimental and quantum chemical calculational studies on 2-[(4-Fluorophenylimino) methyl]-3, 5-dimethoxyphenol, Journal of molecular modeling, **2010**, 16, 577-587.
41- R. G. Parr, R. G. Pearson, Absolute hardness: companion parameter to absolute electronegativity, Journal of the American Chemical Society, **1983**, 105, 7512-7516.
42- O. Benali, L. Larabi, M. Traisnel, L. Gengembre, Y. Harek, Electrochemical, theoretical and XPS studies of 2-mercapto-1-methylimidazole adsorption on carbon steel in 1 M $HClO_4$, Applied surface science, **2007**, 253, 6130-6139.
43- M. Ameer, A. Fekry, Corrosion inhibition of mild steel by natural product compound, Progress in Organic Coatings, **2011**, 71, 343-349.
44- K. Anupama, A. Joseph, Experimental and theoretical studies on Cinnamomum verum leaf extract and one of its major components, eugenol as environmentally benign corrosion inhibitors for mild steel in acid media, Journal of Bio-and Tribo-Corrosion, **2018**, 4, 30.
45- L. O. Olasunkanmi, I. B. Obot, M. M. Kabanda, E. E. Ebenso, Some quinoxalin-6-yl derivatives as corrosion inhibitors for mild steel in hydrochloric acid: experimental and theoretical studies, The Journal of Physical Chemistry C, **2015**, 119, 16004-16019.
46- F. El Hajjaji, H. Greche, M. Taleb, A. Chetouani, A. Aouniti, B. Hammouti, Application of essential oil of thyme vulgaris as green corrosion inhibitor for mild steel in1M HCl, J Mater Environ Sci., **2016,** 7, 566-578.
47- A. Mishra, C. Verma, H. Lgaz, V. Srivastava, M. Quraishi, E. E. Ebenso, Synthesis, characterization and corrosion inhibition studies of N-phenyl-benzamides on the acidic corrosion of mild steel: Experimental and computational studies, Journal of Molecular Liquids, **2018**, 251, 317-332.
48- V. Sastri, J. Perumareddi, Molecular orbital theoretical studies of some organic corrosion inhibitors, Corrosion, **1997**, 53, 617-622.
49- L. C. Murulana, A. K. Singh, S. K. Shukla, M. M. Kabanda, E. E. Ebenso, Experimental and quantum chemical studies of some bis (trifluoromethyl-sulfonyl) imide imidazolium-based ionic liquids as corrosion inhibitors for mild steel in hydrochloric acid solution, Industrial & Engineering Chemistry Research, **2012**, 51, 13282-13299.
50- M. Belghiti, S. Echihi, A. Dafali, Y. Karzazi, M. Bakasse, H. Elalaoui-Elabdallaoui, L. Olasunkanmi, E. Ebenso, M. Tabyaoui, Computational simulation and statistical analysis on the relationship between corrosion inhibition efficiency and molecular structure of some hydrazine derivatives in phosphoric acid on mild

steel surface, Applied Surface Science, **2019**, 491, 707-722.
51- L. H. Madkour, S. Kaya, C. Kaya, L. Guo, Quantum chemical calculations, molecular dynamics simulation and experimental studies of using some azo dyes as corrosion inhibitors for iron. Part 1: Mono-azo dye derivatives, Journal of the Taiwan Institute of Chemical Engineers, **2016**, 68, 461-480.
52- I. Obot, Z. Gasem, Theoretical evaluation of corrosion inhibition performance of some pyrazine derivatives, Corrosion Science, **2014**, 83, 359-366.
53- A. Singh, K. R. Ansari, M. A. Quraishi, Y. Lin, Investigation of Corrosion Inhibitors Adsorption on Metals Using Density Functional Theory and Molecular Dynamics Simulation, in Corrosion Inhibitors, IntechOpen, **2019**.
54- C. Verma, M. Quraishi, E. Ebenso, I. Obot, A. El Assyry, 3-Amino alkylated indoles as corrosion inhibitors for mild steel in 1M HCl: Experimental and theoretical studies, Journal of Molecular Liquids, **2016**, 219, 647-660.
55- I. Lukovits, E. Kalman, F. Zucchi, Corrosion inhibitors-correlation between electronic structure and efficiency, Corrosion, **2001**, 57, 3-8.
56- A. Görling, Density-functional theory beyond the Hohenberg-Kohn theorem, Physical Review A, **1999**, 59, 3359.
57- Y. Karzazi, M. Belghiti, F. El-Hajjaji, B. Hammouti, Density functional theory modeling and monte carlo simulation assessment of N-substituted quinoxaline derivatives as mild steel corrosion inhibitors in acidic medium, J Mater Environ Sci., **2016**, 7, 3916-3929.
58- R. Rahmani, N. Boukabcha, A. Chouaih, F. Hamzaoui, S. Goumri-Said, On the molecular structure, vibrational spectra, HOMO-LUMO, molecular electrostatic potential, UV–Vis, first order hyperpolarizability, and thermodynamic investigations of 3-(4-chlorophenyl)-1-(1yridine-3-yl) prop-2-en-1-one by quantum chemistry calculations, Journal of Molecular Structure, **2018**, 1155, 484-495.
59- P. Mourya, P. Singh, A. Tewari, R. Rastogi, M. Singh, Relationship between structure and inhibition behaviour of quinolinium salts for mild steel corrosion: Experimental and theoretical approach, Corrosion Science, **2015**, 95, 71-87.
60- R. Hsissou, S. Abbout, A. Berisha, M. Berradi, M. Assouag, N. Hajjaji, A. Elharfi, Experimental, DFT and molecular dynamics simulation on the inhibition performance of the DGDCBA epoxy polymer against the corrosion of the E24 carbon steel in 1.0 M HCl solution, Journal of Molecular Structure, **2019**, 1182, 340-351.
61- M. Özcan, I. Dehri, M. Erbil, Organic sulphur-containing compounds as corrosion inhibitors for mild steel in acidic media: correlation between inhibition efficiency and chemical structure, Applied surface science, **2004**, 236, 155-164.
62- O. Dagdag, Z. Safi, H. Erramli, N. Wazzan, L. Guo, C. Verma, E. Ebenso, S. Kaya, A. El Harfi, Epoxy prepolymer as a novel anti-corrosive material for carbon steel in acidic solution: Electrochemical, surface and computational studies, Materials Today Communications, **2020**, 22, 100800.
63- S. Xia, M. Qiu, L. Yu, F. Liu, H. Zhao,, Molecular dynamics and density functional theory study on relationship between structure of imidazoline derivatives and inhibition performance, Corrosion Science, **2008**, 50, 2021-2029.
64- E. Alibakhshi, M. Ramezanzadeh, S. Haddadi, G. Bahlakeh, B. Ramezanzadeh, M. Mahdavian, Persian Liquorice extract as a highly efficient sustainable corrosion inhibitor for mild steel in sodium chloride solution, Journal of cleaner production, **2019**, 210, 660-672.
65- M. K. Awad, M. R. Mustafa, M. M. A. Elnga, Computational simulation of the molecular structure of some triazoles as inhibitors for the corrosion of metal surface, Journal of molecular structure: theochem, **2010**, 959, 66-74.
66- S. K. Saha, P. Banerjee, A theoretical approach to understand the inhibition mechanism of steel corrosion with two aminobenzonitrile inhibitors, RSC Advances, **2015**, 5, 71120-71130.